BMJ Open Diabetes Research & Care

Deletion of GPR21 improves glucose homeostasis and inhibits the CCL2-CCR2 axis by divergent mechanisms

Darren M Riddy ,[1] Helene L Kammoun,[2] Andrew J Murphy,[2] Sanja Bosnyak-Gladovic,[1] Rocio De la Fuente Gonzalez,[1] Jon Merlin ,[1] Mark Ziemann,[3] Stewart Fabb,[1] Tracie L Pierce,[1] Natalie Diepenhorst,[1] Patricia Rueda,[1] Assam El-Osta,[3] Jean-Francois Gautier,[4] Nicolas Venteclef,[4] William N Charman,[1] Arthur Christopoulos,[1] Patrick M Sexton,[1] Roger J Summers,[1] Mark A Febbraio,[1] Philippe Delerive,[5] Christopher J Langmead[1]

To cite: Riddy DM, Kammoun HL, Murphy AJ, *et al*. Deletion of GPR21 improves glucose homeostasis and inhibits the CCL2-CCR2 axis by divergent mechanisms. *BMJ Open Diab Res Care* 2021;**9**:e002285. doi:10.1136/bmjdrc-2021-002285

► Additional supplemental material is published online only. To view, please visit the journal online (http://dx.doi.org/10.1136/bmjdrc-2021-002285).

DMR, HLK and AJM contributed equally.

Received 22 March 2021
Accepted 25 October 2021

Check for updates

© Author(s) (or their employer(s)) 2021. Re-use permitted under CC BY-NC. No commercial re-use. See rights and permissions. Published by BMJ.

For numbered affiliations see end of article.

Correspondence to
Dr Darren M Riddy; darren.riddy@monash.edu and Professor Christopher J Langmead; chris.langmead@monash.edu

ABSTRACT

Introduction A potential role for the orphan G protein-coupled receptor, GPR21, in linking immune cell infiltration into tissues and obesity-induced insulin resistance has been proposed, although limited studies in mice are complicated by non-selective deletion of *Gpr21*.

Research design and methods We hypothesized that a *Gpr21*-selective knockout mouse model, coupled with type 2 diabetes patient samples, would clarify these issues and enable clear assessment of GPR21 as a potential therapeutic target.

Results High-fat feeding studies in *Gpr21*$^{-/-}$ mice revealed improved glucose tolerance and modest changes in inflammatory gene expression. *Gpr21*$^{-/-}$ monocytes and intraperitoneal macrophages had selectively impaired chemotactic responses to monocyte chemoattractant protein (MCP)-1, despite unaltered expression of *Ccr2*. Further genotypic analysis revealed that chemotactic impairment was due to dysregulated monocyte polarization. Patient samples revealed elevated *GPR21* expression in peripheral blood mononuclear cells in type 2 diabetes, which was correlated with both %HbA1c and fasting plasma glucose levels.

Conclusions Collectively, human and mouse data suggest that GPR21 influences both glucose homeostasis and MCP-1/CCL2-CCR2-driven monocyte migration. However, a *Gpr21*$^{-/-}$ bone marrow transplantation and high-fat feeding study in mice revealed no effect on glucose homeostasis, suggesting that there is no (or limited) overlap in the mechanism involved for monocyte-driven inflammation and glucose homeostasis.

Significance of this study

What is already known about this subject?

- GPR21 was proposed as a novel target to treat type 2 diabetes.
- Deletion of *Gpr21* using traditional methods affected *Rabgap1* expression confounding data interpretation and novelty.

What are the new findings?

- CRISPR-Cas9 generated *Gpr21*-deficient mouse displays improved glucose tolerance.
- Phenotype not replicated in selectively deleted *Gpr21* myeloid cells.
- *Gpr21*$^{-/-}$ monocytes and IP macrophages display selectively impaired chemotaxis.

How might these results change the focus of research or clinical practice?

- No, or limited, overlap in the mechanism involved for monocyte-driven inflammation and glucose homeostasis.
- Inhibition of GPR21 could yield improvements in both obesity-induced insulin resistance and in diseases in which CCR2-driven inflammation is key, opening up a number of therapeutic indications in which GPR21 antagonists might be effective.

INTRODUCTION

Chronic, low-grade inflammation is part of the pathogenesis of obesity-induced insulin resistance that manifests as immune cell infiltration into adipose tissue.[1–5] The population of metabolic and immune cells, including adipocytes and macrophages, paralleled by activation of various proinflammatory receptors and signaling pathways, posits a mechanistic link between insulin resistance and inflammation. However, other evidence suggests no causative link, and that improvements in insulin resistance and inflammation occur via separate mechanisms.[6 7]

Over 30 G protein-coupled receptors (GPCRs) have been implicated in the development and progression of type 2 diabetes (T2D), including orphan receptors.[8] However, only the glucagon-like peptide-1 receptor (GLP-1R) has been successfully targeted therapeutically.[9] Of these orphan

BMJ Open Diab Res Care: first published as 10.1136/bmjdrc-2021-002285 on 15 November 2021. Downloaded from http://drc.bmj.com/ on April 27, 2024 by guest. Protected by copyright.

GPCRs, there have been limited studies on GPR21, a receptor widely expressed in metabolically important tissues, including skeletal muscle, brown adipose tissue and hypothalamus.[10 11] Notably, GPR21 is expressed at moderate levels in immune cells, including monocytes and various macrophage populations.[11]

Two independent studies of *Gpr21* knockout mice revealed a robust improvement in glucose tolerance and insulin sensitivity after chronic high-fat diet (HFD),[11 12] due to reduced tissue inflammation and impaired monocyte and macrophage migration into adipose tissue. Since these promising findings, controversy has arisen around the etiology of the phenotype. A subsequent study suggested that the metabolic improvements were due to disruption of *Rabgap1*, which encodes for the RAB GTPase activating protein 1 and is the gene within which *Gpr21* is nested.[13] The authors of this study speculated that insertion of a LacZ-Neo cassette into the *Gpr21* gene during the generation of the transgenic mouse disrupted *Rabgap1* expression, and it is this effect, rather than disruption of *Gpr21*, that underlies the metabolic phenotype. This discrepancy in the knockout phenotypes, together with the paucity of other studies on GPR21, demonstrates a need to better understand function of the receptor with improved mouse models and human data.

In an attempt to reconcile differences in the literature, and understand potential roles for GPR21 as a therapeutic target in metabolic diseases, we developed a novel *Gpr21* knockout mouse using CRISPR-Cas9 technology for phenotyping in HFD feeding studies, using both whole-body knockout and bone marrow transplant (BMT) models. We also investigated differential expression of *GPR21* in control and patients with T2D, and RNA-Seq analysis of, and migration assays with, *Gpr21*$^{-/-}$ CD11b^{+} bone marrow monocytes (BMMs).

In contrast with the original *Gpr21*$^{-/-}$ mouse strain,[11] our CRISPR *Gpr21*$^{-/-}$ mice had unaltered *Rabgap1* expression, yet still displayed improved glucose tolerance when fed HFD. Absence of *Gpr21* caused a selective reduction in inflammatory markers in adipose tissue and liver, and *Gpr21*$^{-/-}$ CD11b^{+} BMMs and intraperitoneal (IP) macrophages exhibited selective impaired chemotactic responses to monocyte chemoattractant protein-1 (MCP-1; CCL2), despite unaltered CCR2 expression. Further analysis revealed that this impaired inflammatory response is due to dysregulated monocyte polarization.

However, the improved metabolic phenotype of *Gpr21*$^{-/-}$ was not preserved in the BMT model, suggesting that although GPR21 influences both glucose homeostasis and monocyte function, the two phenotypes are not intrinsically linked. We speculate that due to the compelling effects on monocyte function, GPR21 might be a promising therapeutic target for CCR2-driven inflammatory conditions.

RESEARCH DESIGN AND METHODS

Generation of *Gpr21*$^{-/-}$ animals and ethics

CRISPR *Gpr21*$^{-/-}$ mice (containing a 3.8 kb deletion of exon 2 of *Gpr21*) were generated following backcrossing onto the C57BL/6J background for more than seven generations (Australian Phenomics Network, Melbourne, Australia). Guide RNA target sites flanking exon ENSMUSE00000450988 of the *Gpr21* gene were designed using http://crispr.mit.edu/ (online supplemental table 1). Complementary oligonucleotides of target sites were annealed and cloned into BbsI (NEB) digested plasmid pX330-U6-Chimeric_BB-CBh-hSpCas9 (Addgene plasmid #42230). Single guide RNAs (sgRNAs) were generated using the HiScribe T7 Quick High Yield RNA Synthesis Kit (NEB) according to the manufacturer's instructions (online supplemental table 1). RNAs were purified (RNeasy Mini Kit, Qiagen, Germany) and Cas9 mRNA (Sigma-Aldrich, Castle Hill, Australia, 30 ng/µL) and sgRNAs (15 ng/µL) were microinjected into the cytoplasm of C57BL/6J zygotes at the pronuclei stage. Zygotes were transferred into the uterus of pseudo pregnant F1 females. Deltagen mice were obtained from Deltagen (USA) as per previous works.[11 12]

Animal studies were conducted in accordance with the Australian Code of Practice for the Care and Use of Animals for Scientific Purposes, and study protocols reviewed and approved by the Monash University (Clayton, VIC, Australia), the Monash University Research Ethics Committee (Clayton, VIC, Australia), Baker Heart and Diabetes Institute (Melbourne, VIC, Australia) and the Alfred Medical Research and Education Precinct Ethics Committee (Melbourne, VIC, Australia). Breeding and experimental procedures of these animals were in accordance with MARP/2015/012/BC, MARP/2015/0140/Exp/Cowley/MA, MIPS/2016/15/(DARREN RIDDY) and 5477HK. To avoid hormonal effects, only male mice were used for experiments. Mice were housed in a 12-hour light, 12-hour dark cycle with food and water ad libitum. For feeding studies, mice were fed either normal chow (NC) (8.9% energy from fat; Specialty Feeds, Glen Forrest, WA, Australia) or HFD (60% energy from fat; SF16-048, Specialty Feeds,). Diets started at week 1 of the study. For genotyping, the primers (Gene Works, Melbourne, Australia) used are described in online supplemental table 2.

Human ethics

Collection and use of human blood samples was conducted according to the guidelines and approval of the Monash University (Clayton, Australia) and the Monash University Research Ethics Committee (Parkville, Australia; 2021-21414-57552). Blood was obtained from donation by vein puncture of human volunteers from the Victorian Blood Donor Registry, or from buffy coat preparations from the Australian Red Cross blood service (Melbourne, Australia, agreement number 18-08VIC-11). Blood was collected by written consent for the purposes of research. Adipose tissue and peripheral blood

BMJ Open Diab Res Care: first published as 10.1136/bmjdrc-2021-002285 on 15 November 2021. Downloaded from http://drc.bmj.com/ on April 27, 2024 by guest. Protected by copyright.

mononuclear cell (PBMC) clinical samples used were obtained from two studies described in previous works ([14]2016; NCT02368704) and ([15]2019; NCT02671864). Both studies were conducted in accordance with the principles of the Declaration of Helsinki, with informed consent.

Bone marrow isolation and transplantation

Bone marrow (BM) was isolated from the femur and tibia of wild-type (n=3) and *Gpr21*$^{-/-}$ (n=3) mice by flushing of the BM cavity with phosphate buffered saline (PBS). Cells were washed in RPMI and counted using a hematology analyzer Xs-1000i (Sysmex, Germany). Cells (~3×10^6 cells) were injected into the tail vein of 8-week-old male irradiated (2×5.5 Gy) wild-type C57BL/6J mice. Mice were allowed 5 weeks for reconstitution of donor BM and recovery.

Mouse and human cell isolations and function assays

BMMs were isolated as described in previous work.[6] CD11b$^+$ monocytes were isolated by negative selection and magnetic bead separation method (Miltenyi Biotech, Germany) according to manufacturer's instructions. IP macrophages were obtained by flushing the IP space with 0.9% PBS. Human CD14$^+$ PBMCs were isolated as described in previous work.[16] Ex vivo migration of human CD14$^+$, mouse CD11b$^+$ BMMs and IP macrophages were performed as described previously.[16] Monocyte adhesion and shape change polarization assays were performed as described in previous works[17 18] and use of F-actin staining.

Ex vivo migration of CD11b$^+$ BM monocytes and IP macrophages measured by chemotaxis

Chemotaxis assays were performed using HTS-transwell inserts (Sigma-Aldrich, Castle Hill). A volume of 150 µL of chemoattractant (monocyte chemoattractant protein-1; MCP-1, monocyte chemoattractant protein-2; MCP-2, monocyte chemoattractant protein-3; MCP-3, monocyte inhibitory protein-1α; MIP1α) in serum-free growth medium was added to the bottom chamber of the insert. In the top chamber, 50,000 cells resuspended in 50 µL serum-free growth medium were added. A negative control using vehicle and positive control using 10% fetal bovine serum (FBS; replicate wells) were included in each assay. Once the samples were prepared the plates were incubated for 3 hours, at 37°C with 5% CO_2. Following the incubation, transwells were removed and the plates dried before fixing the cells with formalin solution containing Hoechst 33258 (Sigma-Aldrich) for nuclei staining. Wells were imaged using an InCell Analyzer 2000 (GE Healthcare, Little Chalfont) and number of cells quantified using Image J V.1.50b (NIH, US).

Metabolic parameters

MRI, oral glucose (OGTT), and IP insulin tolerance tests (IPITT) were performed as described previously.[6] Plasma insulin concentrations were measured using a Mouse Ultrasensitive Insulin ELISA kit (ALPCO, Salem, New Hampshire, USA) according to manufacturer's instructions.

Tissue processing and FACS analysis

Epididymal fat pads were rinsed in PBS and minced in FACS buffer (PBS containing 1% bovine serum albumin (BSA)). Adipocytes and stromal vascular cells were prepared from collagenase-digested adipose tissue. In brief, tissue homogenates were incubated in 1 mL PBS supplemented with 0.5% BSA and 3 mL collagenase II digest solution using a rotational shaker for 20 min at 37°C. All samples were washed twice with PBS and passed through a 70 µm filter. The suspension was centrifuged at 500×g for 10 min at 4°C and resuspended in FACS buffer. FACS analysis of stromal vascular fraction (SVF) for immune cell content were performed using fluorescently conjugated antibodies to various markers, including PB-CD45, APC-CD115, Percp-Gr1, APCCy7-CD3, FITC-CD19, PECy7-F4/80, G05-CD206, PE-NK1.1, and Percp-CD11c (Australian Biosearch, Wangara, WA, Australia). For mouse CD11b$^+$ BM monocytes, cells were isolated from both wild-type and *Gpr21*$^{-/-}$ animals as described above. Cell populations were characterized using fluorescently conjugated antibodies to Ly6C, Ccr2 and Cx3cr1 (Australian Biosearch, Wangara, WA, Australia). Content was measured by use of a BD FACS LSRFortessa (BD Biosciences, Singapore). Data were analyzed using FlowJo V.10 (LLC, Ashland, Oregon, USA). All data are expressed as % cell population gated from CD45 + cells. Whole blood and liver were prepared as above but in the absence of collagenase.

Gene expression and RNA sequencing

Knockdown of *GPR21* in CD14$^+$ PBMCs was achieved using lentiviral shRNA using scrambled or *GPR21* specific sequence with a multiplicity of infection (MOI) of 10 (with ~60% efficiency). Cells were sorted by selecting sytox red$^-$/GFP$^+$ cells. mRNA extraction and gene expression analysis were performed as described in previous work.[16] Primers (Gene Works, Melbourne, Australia) used for the study are described in online supplemental table 3.

Mouse CD11b$^+$ RNA was isolated from Trizol homogenates using the Direct-zol RNA MiniPrep Kit (Zymo Research, California, USA). RNA depletion and library construction were performed using NEBNext rRNA Depletion Kit and NEBNext UltraTM Directional RNA Library Prep Kit for Illumina (NEB, USA). Library QC was performed by MultiNA Bioanalyzer (Shimadzu Japan) and pooled to equimolar concentration. Libraries underwent Illumina single read sequencing (AGRF, Melbourne, Australia) using HiSeq v4 reagents to generate 100 bp reads.

Data analysis and bioinformatics

Chemotaxis, FACS (fluorescently conjugated antibodies shown in online supplemental table 4) and gene expression analysis were performed as described in previous

BMJ Open Diab Res Care: first published as 10.1136/bmjdrc-2021-002285 on 15 November 2021. Downloaded from http://drc.bmj.com/ on April 27, 2024 by guest. Protected by copyright.

work.[16] Polarization data are expressed as the percentage of monocytes with >1.5-pixel distance. Bioinformatic analysis were performed as described in previous works.[19–25] Ternary expression diagrams were generated using the ggtern package and heatmaps were generated using the gplots package in R. Experiments were analyzed using FlowJo V.10 (LLC, Ashland, Oregon, USA) and Prism V.9.0a (GraphPad Software, San Diego, California, USA).

Statistical analysis

In all cases, data are shown and mean+SEM, with the number of replicates indicated within the figure legend. In most cases, statistical significance was deemed by two-way analysis of variance (ANOVA) with Tukey's post hoc multiple comparison test compared with wild-type animals fed NC. *Rabgap1* expression was deemed significant by multiple t-test with Holm-Sidak multiple comparison test, compared with wild-type. Gene expression data were deemed significant using one-way ANOVA with Dunnett's multiple comparison test compared with wild-type NC (*) or HFD (#).

RESULTS

Previous *Gpr21*$^{-/-}$ mouse studies have been potentially confounded by effects on *Rabgap1*, the gene in which *Gpr21* is nested.[11–13] Using CRISPR-Cas9 technology, we developed a new knockout, termed CRISPR *Gpr21*$^{-/-}$. Figure 1A compares the strategies used to generate this mouse compared with the original *Gpr21*$^{-/-}$ knockout mouse.[11 12] We confirm that *Rabgap1* is significantly altered in metabolic tissues and immune cells of the original knockout mouse, specifically downstream of *Gpr21* (figure 1B–D), while deletion of *Gpr21* in our new model did not significantly alter *Rabgap1* expression (figure 1E–G).

Having established a clean genetic knockout of *Gpr21*, we explored the suitability of this new model to study the effects of mice fed HFD. First, we noted no significant difference in body weight of *Gpr21*$^{-/-}$ mice compared with wild-type littermate controls prior to placing mice on their respective diets (online supplemental figure 1a, n=6–12). After the 16-week feeding period, wild-type controls fed HFD displayed the expected increased body weight compared with NC fed animals (figure 2A,B, n=6–12). Interestingly, *Gpr21*$^{-/-}$ animals gained less weight on a HFD compared with control mice and, over the duration of the experiment, gained the same amount of weight irrespective of whether they consumed HFD or NC (figure 2B, n=6–12). Although no genotype difference in glucose tolerance was evident after 6 weeks of HFD (online supplemental figure 1a–d, n=6–12), OGTTs after 12 weeks revealed an improvement in glucose handling in *Gpr21*$^{-/-}$ animals fed HFD compared with controls (figure 2C,D, n=6–12). However, fasting plasma glucose levels appeared not to be influenced by *Gpr21* deletion (figure 2E, n=6–12).

At the conclusion of the study, key metabolic tissues were collected and analyzed for changes in the expression of key inflammatory genes. HFD promoted the expression of *Ccr2*, *Ccl2*, *Il1β*, and *Nlrp3* in the epididymal WAT (eWAT) and liver of wild-type animals, which was in part lower in the *Gpr21*$^{-/-}$ mice (figure 2F,G, n=6–12). However, histologic analysis revealed no genotypic differences in lipid droplet number and size (liver) and adipocyte area and circularity (eWAT; online supplemental figure 1e–f).

Given the reduction in *Ccr2* expression in eWAT and liver, we explored the potential role of GPR21 in immune cells, specifically monocytes. However, before investigating any potential functional differences, we profiled BMMs isolated from wild-type and *Gpr21*$^{-/-}$ animals by FACS to check that the isolation procedure yielded similar populations of cells. Markers for phagocytosis and proinflammatory monocytes (CD11b^{+} Ly6C^{high} CCR2^{high} CX3CR1^{low}), proinflammatory (CD11b^{+} Ly6C^{medium} CCR2^{high} CX3CR1^{low}), and patrolling tissue repair anti-inflammatory monocytes (CD11b^{+} Ly6C^{low} CCR2^{low} CX3CR1^{high}[26]) revealed no genotypic differences between the populations isolated (figure 3A,B, n=5). MCP-1 (1–1000 ng/mL) robustly stimulated chemotaxis in wild-type CD11b^{+} monocytes with a classical bell-shaped curve, a response that was significantly blunted in *Gpr21*$^{-/-}$ CD11b^{+} monocytes (figure 3C, n=4–9), despite unchanged cell-surface expression of Ccr2 (figure 3D, n=4). The effect on MCP-1 function was highly specific, as *Gpr21*$^{-/-}$ CD11b^{+} monocytes responded to chemotactic gradients of MCP-3 and macrophage inflammatory protein (MIP)-1α in an identical manner to those isolated from wild-type animals, ruling out generalized defects in chemotaxis (figure 3E,F, n=3–4). A similar reduction in chemotaxis to MCP-1 was observed in macrophages isolated from the intraperitoneal space of the same animals (figure 3G, n=4–9).

To probe deeper into the role of GPR21 on monocyte function, transcriptomic analysis was performed on CD11b^{+} BMMs isolated from both wild-type and *Gpr21*$^{-/-}$ mice. Prior to differential expression analysis, filtering was performed to remove genes with <10 reads. From the initial 48,526 genes, 14,512 were selected for further analysis (online supplemental figure 2a and online supplemental table 5). Analysis revealed 324 differentially expressed genes (DEGs) at a false detection rate (FDR)<0.05, 81<0.01, and 49<0.001 (online supplemental figure 2b). Of the 324 DEGs, 127 were upregulated and 197 downregulated (online supplemental figure 2c); the top 50 regulated genes are shown in a volcano plot in figure 4A and as a heatmap (online supplemental figure 2d and online supplemental tables 6 and 7). Gene set enrichment analysis (GSEA) using sets from Reactome identified an increase in toll-like receptor trafficking, circadian expression, and the NOD, LRR and pyrin domain-containing protein 3 (NLRP3) inflammasome (online supplemental figure 2e), in *Gpr21*$^{-/-}$ compared with

BMJ Open Diab Res Care: first published as 10.1136/bmjdrc-2021-002285 on 15 November 2021. Downloaded from http://drc.bmj.com/ on April 27, 2024 by guest. Protected by copyright.

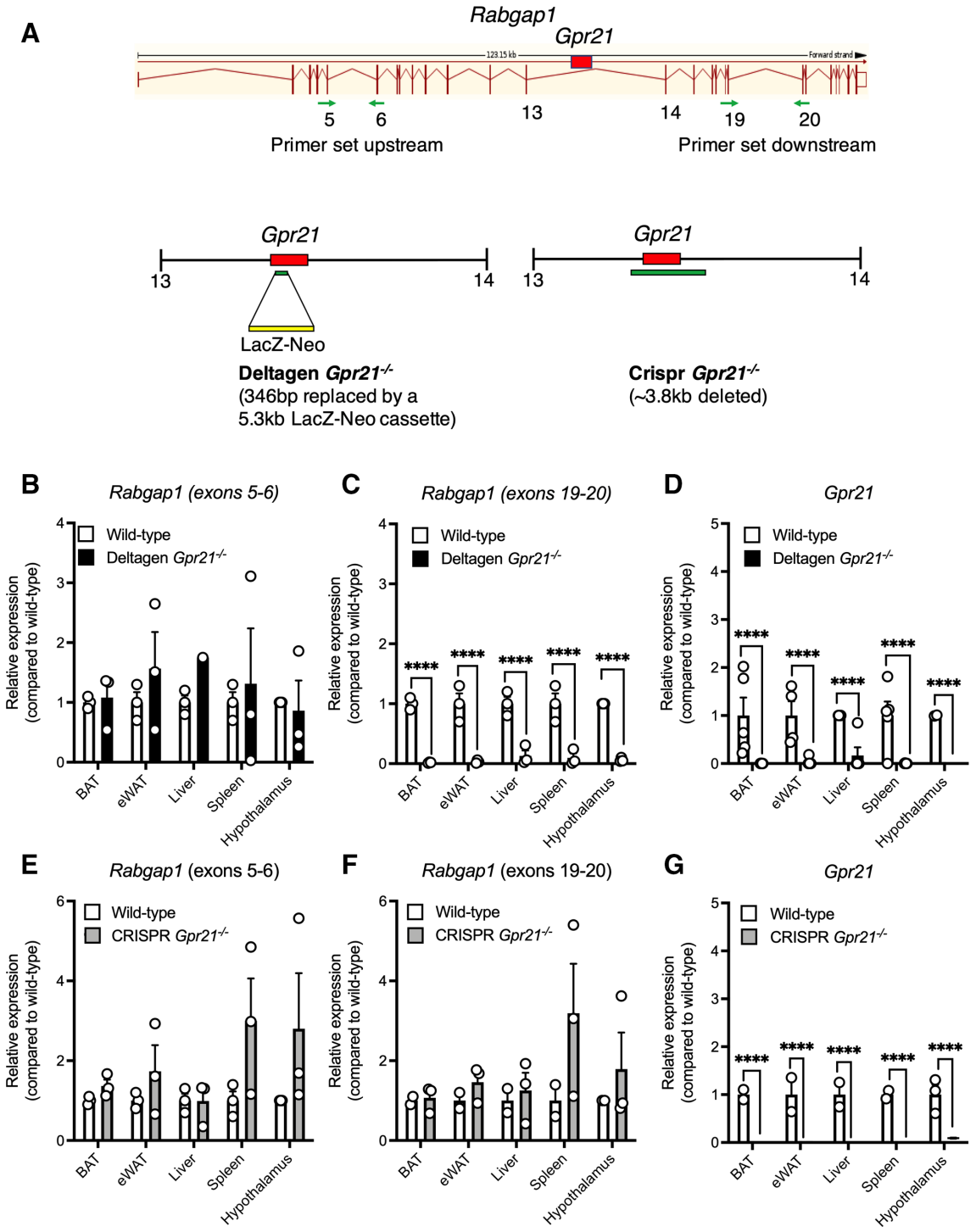

Figure 1 *Gpr21* deletion does not affect *Rabgap1* expression. (A) Comparison of the regions deleted in the published Deltagen and the CRISPR knockout model used within this study. Relative expression of (B and E) *Rabgap1* measured upstream of *Gpr21* (exons 5–6), (C and F) *Rabgap1* measured downstream of *Gpr21* (exons 19–20), and (D and G) *Gpr21* in various tissues from wild-type (white bars), Deltagen (black bars) and CRISPR (gray bars) $Gpr21^{-/-}$ animals, respectively. All data are presented as mean+SEM (n=3–4). Multiple t-tests with Holm-Sidak multiple comparison test, ****p<0.0001, compared with wild type. WAT, white adipose tissue.

wild-type mice, whereas decreases were observed for collagen formation, extracellular matrix organization and degradation, and nitric oxide signaling (online supplemental figure 2e). GSEA enrichment plots revealed regulation of pathways clearly linked to the phenotype of $Gpr21^{-/-}$ mice, including inflammatory response, monocyte chemotaxis, and GPCR signaling (online supplemental figure 2f,g). Focused analysis of selected genes associated with monocyte adhesion and polarization, including integrins, revealed a downregulation of *Itgb3*, *Itga2b*, *Itgab2l* and *CD9* in $Gpr21^{-/-}$ $CD11b^{+}$ BM compared with wild type (figure 4B). To

BMJ Open Diab Res Care: first published as 10.1136/bmjdrc-2021-002285 on 15 November 2021. Downloaded from http://drc.bmj.com/ on April 27, 2024 by guest. Protected by copyright.

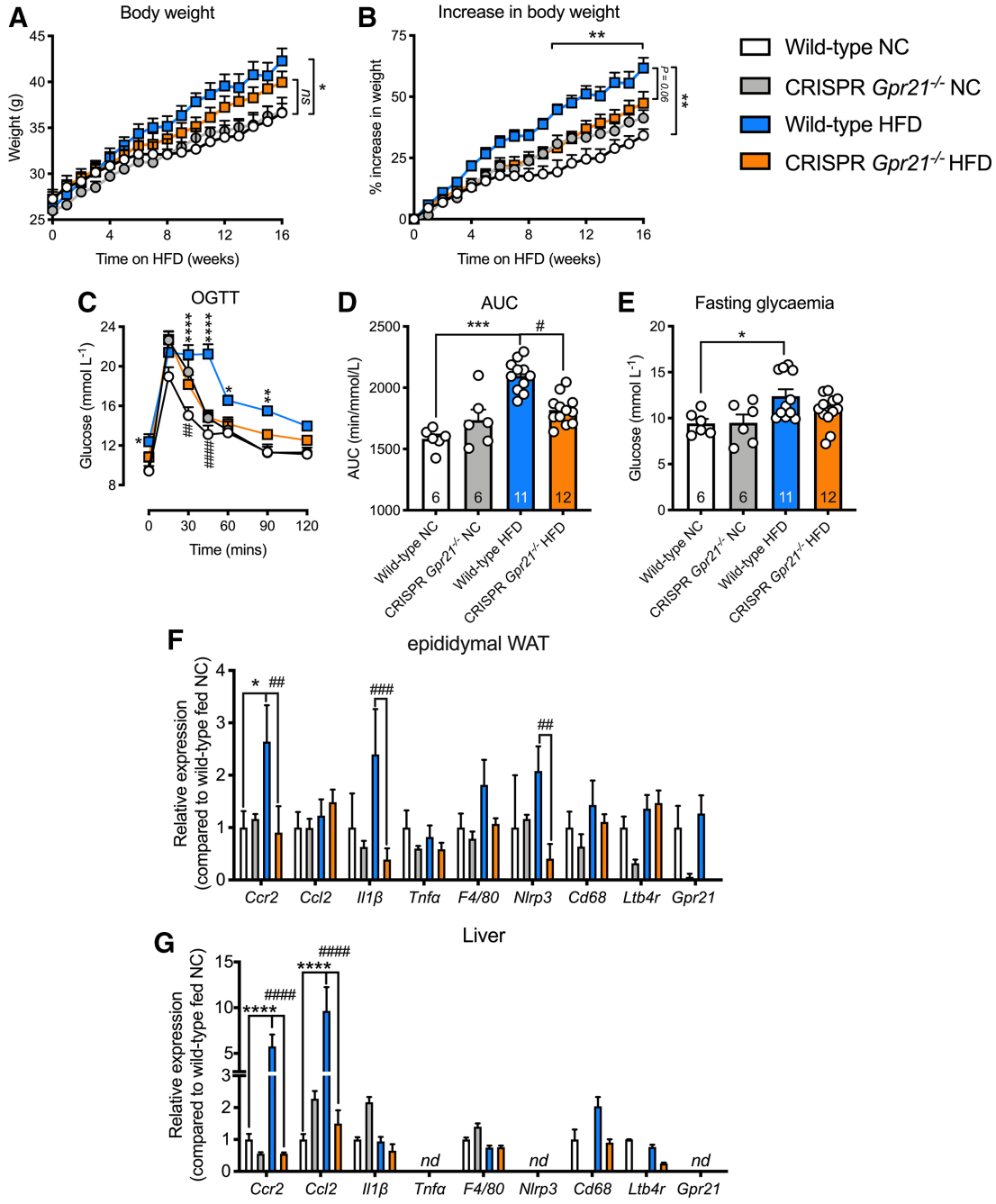

Figure 2 Whole-body deletion of *Gpr21* reveals improved glucose handling. Changes in (A) body weight (BW) (g), (B) BW % of wild-type and *Gpr21*$^{-/-}$ mice on normal chow (NC) and high-fat diet (HFD). Week 12 (C) oral glucose tolerance test (OGTT; 3 g/kg lean), (D) area under the curve (AUC), (E) fasting glycemia, relative gene expression of inflammatory and energy expenditure markers in (F) epididymal white adipose tissue (WAT) and (G) liver, as measured by qPCR (*n/d*=not detected). All data are presented as mean+SEM (n=6–12, unless otherwise stated). Statistical significance was determined by two-way analysis of variance with Tukey's multiple comparison test compared with wild-type NC, with *p<0.05, **p<0.01, ***p<0.001, and ****p<0.0001 deemed significant and compared with wild-type HFD with $^{\#}$p<0.05, $^{\#\#}$p<0.01, $^{\#\#\#}$p<0.001, and $^{\#\#\#\#}$p<0.0001 deemed significant.

explore the mechanistic link between these changes and the functional phenotype of *Gpr21*$^{-/-}$ CD11b^{+} BMMs, we performed cell adhesion and polarization assays. Wild-type and *Gpr21*$^{-/-}$ CD11b^{+} BMMs had a similar capacity to adhere to fibronectin plates following treatment with MCP-1 (100 ng/mL; figure 4C, n=7); however, *Gpr21*$^{-/-}$ CD11b^{+} BMMs displayed significantly impaired polarization-induced morphological changes, compared with wild-type cells (figure 4D,E, n=7), which likely underpins the impaired chemotactic response.

To investigate the translational relevance of GPR21 as a therapeutic target in metabolic disorders, tissue and blood samples from patients with T2D and healthy

BMJ Open Diab Res Care: first published as 10.1136/bmjdrc-2021-002285 on 15 November 2021. Downloaded from http://drc.bmj.com/ on April 27, 2024 by guest. Protected by copyright.

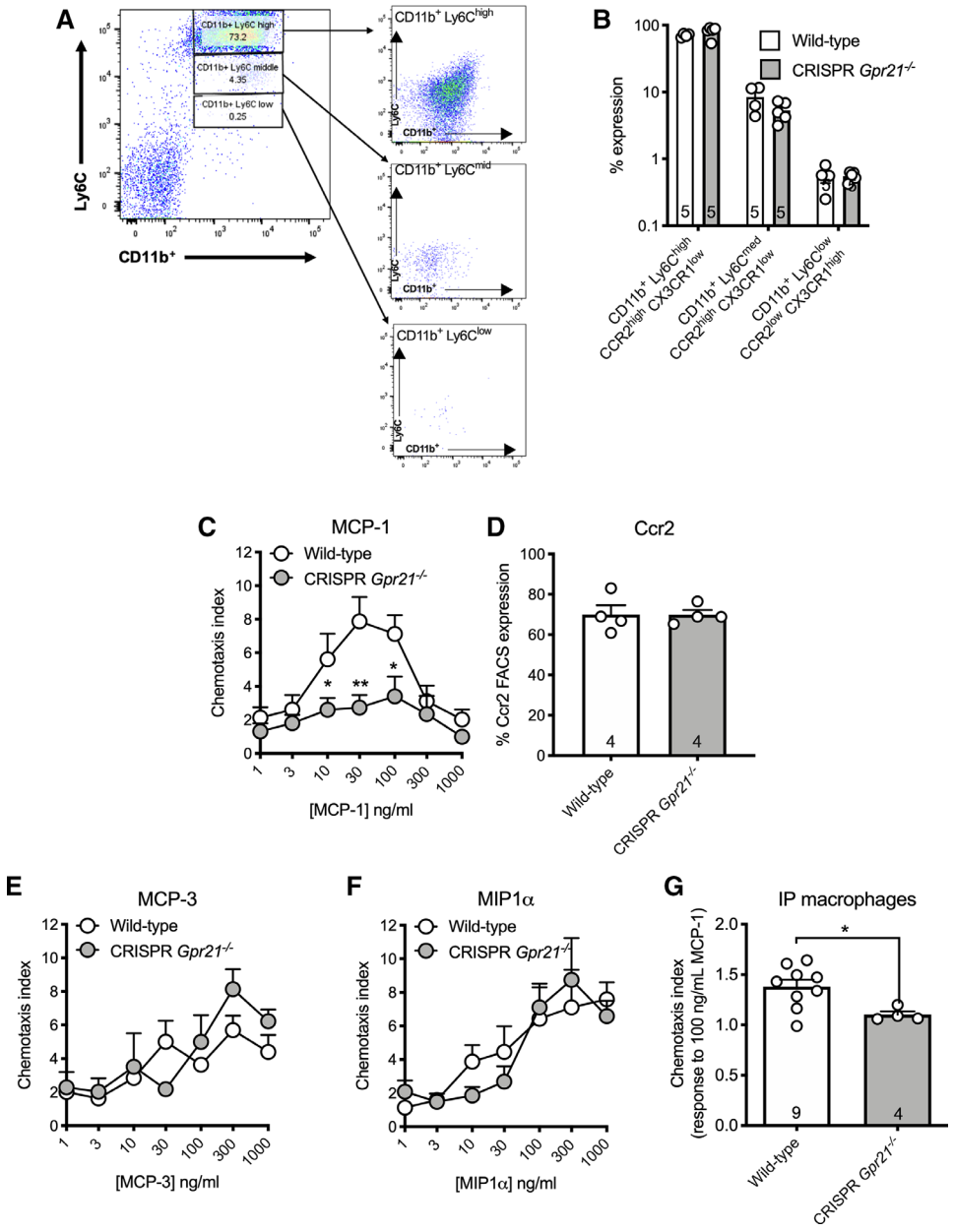

Figure 3 Deletion of *Gpr21* does not alter the CD11b$^+$ bone marrow (BM) monocyte population but selectively inhibits monocyte chemoattractant protein-1 (MCP-1) driven monocyte migration. Representative FACS analysis of CD11b$^+$ BM monocytes isolated from (A) wild-type and *Gpr21*$^{-/-}$ animals as measured by CD11b$^+$ and Ly6C expression and (B) comparative quantification of cell populations. Chemotaxis of (C) CD11b$^+$ BM monocytes isolated from wild-type and *Gpr21*$^{-/-}$ animals in response to MCP-1. Relative gene expression of Ccr2 in (D) CD11b$^+$ BM monocytes, as measured by FACS. Chemotaxis of CD11b$^+$ BM monocytes isolated from wild-type and *Gpr21*$^{-/-}$ animals in response to (E) MCP-3 and (F) macrophage inflammatory protein-1α (MIP1α). Chemotaxis of (G) intraperitoneal (IP) macrophages isolated from wild-type and *Gpr21*$^{-/-}$ animals in response to MCP-1. All data are presented as mean+SEM (n=7, otherwise stated). Statistical significance was determined by Student's t-test, or two-way analysis of variance with Tukey's multiple comparison test compared with wild type, with *p<0.05, and **p<0.01 deemed significant.

controls were assessed. mRNA levels for both the proinflammatory MCP-1 (*CCL2*) and *GPR21* were higher in WAT of patients with T2D compared with matched controls (figure 5A,B; n=8–16). Furthermore, there was a significant correlation between WAT *GPR21* expression and %HbA1c levels in patients with T2D (figure 5C; *p<0.015, n=24; mean %HbA1c 7.4±1.2;[15] 2019; NCT02671864). As increased *Gpr21* expression in eWAT from mice fed HFD is found in the SVF, but not the adipocyte population (figure 5D; **p<0.007, n=8), we extended patient profiling to CD14$^+$ PBMCs and found that *GPR21* expression was significantly higher in CD14$^+$ cells from patients with T2D (figure 5E; n=26–82), which also correlated with fasting plasma glucose (figure 5F; **p<0.005, n=86). Emphasizing a link between MCP-1 and GPR21 in CD14$^+$ PBMCs from healthy blood donors,

BMJ Open Diab Res Care: first published as 10.1136/bmjdrc-2021-002285 on 15 November 2021. Downloaded from http://drc.bmj.com/ on April 27, 2024 by guest. Protected by copyright.

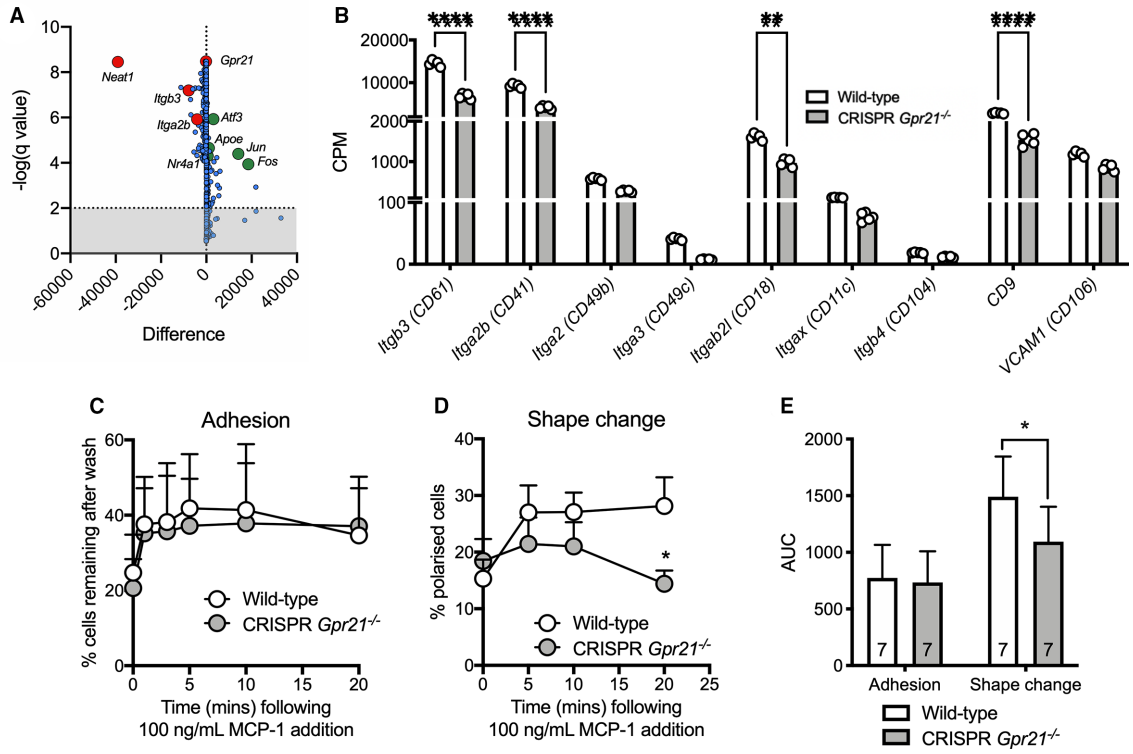

Figure 4 RNA-Seq analysis of CD11b$^+$ bone marrow (BM) monocytes suggests downregulation of integrin expression and impaired monocyte shape change (polarization). Volcano plot (A) of the top 1450 genes (ordered by false detection rate), with genes of interest highlighted (large differences and high significance; top left, downregulated; top right, upregulated). Analysis of integrin expression (B) in RNA-Seq dataset. Time course of (C) adhesion and (D) shape change of CD11b$^+$ BM monocytes isolated from wild-type and *Gpr21*$^{-/-}$ animals in response to 100 ng/mL monocyte chemoattractant protein-1 (MCP-1), and (E) area under the curve (AUC). All data are presented as mean+SEM (n=5–7, otherwise stated). Statistical significance was determined by multiple t-tests with Holm-Sidak multiple comparison test, ****p<0.0001, compared with wild type, or two-way analysis of variance with Tukey's multiple comparison test compared with wild type, with *p<0.05 and **p<0.01 deemed significant. Bioinformatics analysis was performed as described in the Research design and methods section.

we observed a correlation between expression of *GPR21* and *CCR2B*, the primary receptor for MCP-1 (figure 5G, *p<0.017, n=8). Finally, to explore a possible functional link between these genes we used a lentiviral-mediated knockdown of *GPR21* in CD14$^+$ PBMCs isolated from healthy donors, which resulted in significantly impaired chemotaxis (figure 5H, n=7). Collectively, these clinical data provide evidence linking GPR21 to both glucose homeostasis and regulation of the MCP-1/CCL2-CCR2 axis.

Given that convergent mouse and human data suggest GPR21 both plays a role in glucose homeostasis and is a major regulator of MCP-1/CCR2-driven chemotaxis and inflammation, we sought to determine the extent to which these two phenotypes were linked. To test whether the protective effect on glucose homeostasis was due solely to loss of *Gpr21* in cells of the hemopoietic lineage, we performed a bone marrow transplant (BMT; experimental overview figure 6A, n=6–12), followed by HFD feeding and assessments measured as per the whole-body study. All animals placed on HFD increased their body weight and fat mass, and decreased their lean mass (figure 6B–D, n=6–12). Initially, *Gpr21*$^{-/-}$ recipient animals on HFD gained weight at a faster rate than wild-type controls (figure 6B–D, n=6–12), although this difference was lost after 8 weeks. Although 25 weeks of HFD modestly increased fasting plasma glucose levels in wild-type mice, there was no impairment in glucose handling (figure 6E–G, n=6–12). *Gpr21*$^{-/-}$ recipient animals on NC also displayed significantly higher fasting plasma glucose than wild-type controls (figure 6G, n=6–12). All groups displayed increased insulin levels in response to glucose challenge, and *Gpr21*$^{-/-}$ recipient mice had lower levels of plasma insulin both before and during GTTs compared with their respective wild-type controls (both for NC and HFD fed mice; figure 6H, n=11). No improvement in insulin tolerance was observed over a 2-hour time course and as measured by AUC (figure 6I,J, n=6–12). Interestingly, isolated *Gpr21*$^{-/-}$ CD11b$^+$ BMMs at the end of the study failed to respond to 100 ng/mL MCP-1 compared with wild-type (figure 6K), confirming the chemotactic phenotype described above (figure 2C). Although *Gpr21*$^{-/-}$ BMT recipient animals did not display improved glucose handling, tissue profiling revealed similar changes in pro-inflammatory gene expression as seen in the whole-body knockout study. HFD increased *Ccl2*, *Ccr2*, *Tnfα*, *F4/80*, and *Cd68* expression in eWAT and liver compared with wild-type animals fed NC; the

BMJ Open Diab Res Care: first published as 10.1136/bmjdrc-2021-002285 on 15 November 2021. Downloaded from http://drc.bmj.com/ on April 27, 2024 by guest. Protected by copyright.

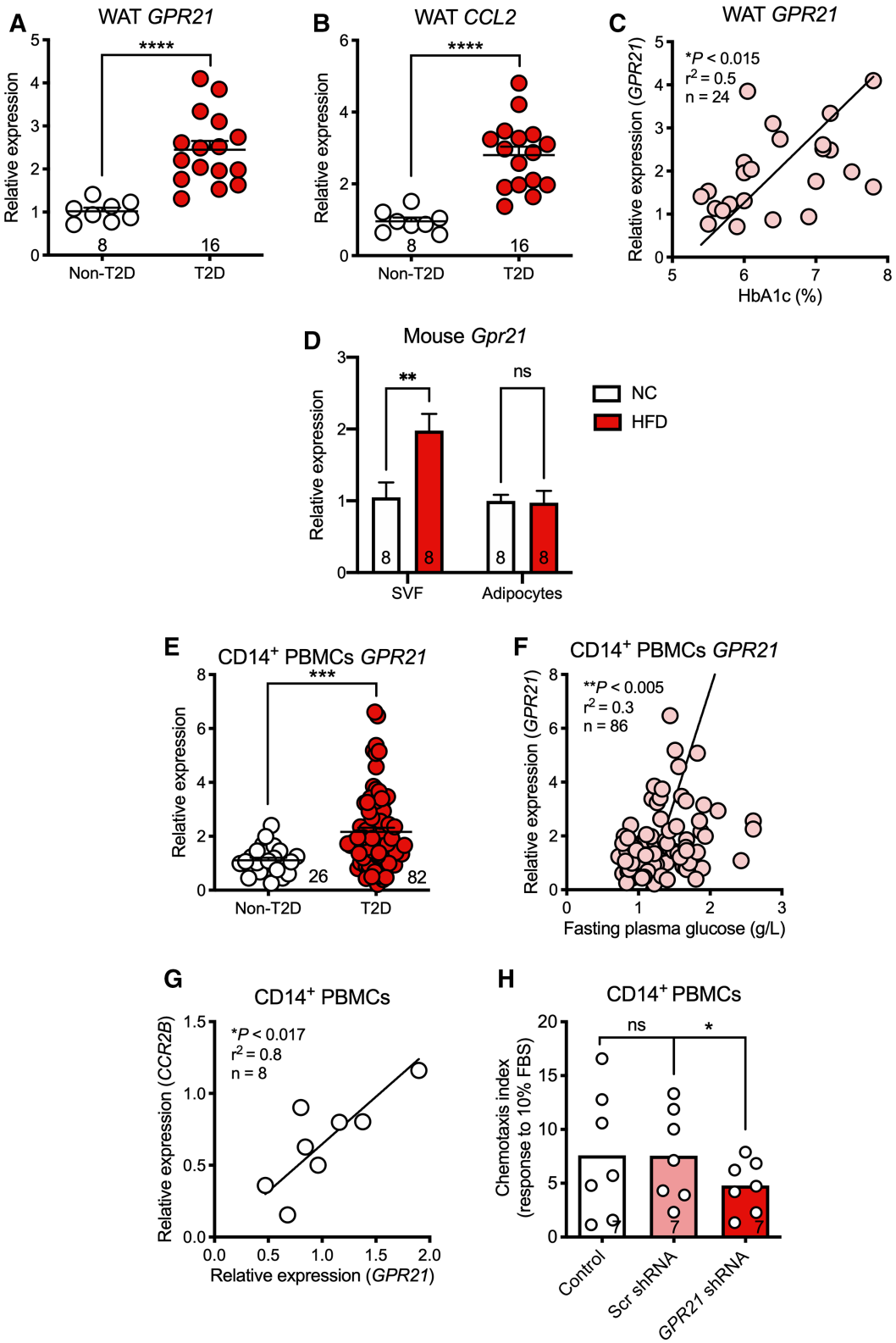

Figure 5 *GPR21* is upregulated in white adipose tissue (WAT) and immune cells of patients with type 2 diabetes (T2D). *GPR21* (A) and *CCL2* (B) mRNA levels are upregulated in WAT of patients with T2D, and *GPR21* expression correlates with %HbA1c (C). Expression of mouse *Gpr21* is increased in the stromal vascular fraction (SVF) of mice fed high-fat diet (HFD), but not in adipocytes (D). Expression of *GPR21* (E) is upregulated in CD14$^+$ peripheral blood mononuclear cells (PBMCs) and correlates with (F) fasting plasma glucose levels in patients with T2D. Expression of (G) *GPR21* in PBMCs correlates with *CCR2B* expression and (H) knockdown by selective *GPR21*-LV-shRNA reduces monocyte migration in response to 10% FBS. All data are expressed as mean+SEM. Replicates are shown on each panel. Statistical significance was determined by Student's t-test, one-way analysis of variance (ANOVA) with Tukey's multiple comparison test compared with wild-type control, or two-way ANOVA with Sidak's multiple comparison, with *p<0.05 deemed significant. FBS, fetal bovine serum; NC, normal chow.

BMJ Open Diab Res Care: first published as 10.1136/bmjdrc-2021-002285 on 15 November 2021. Downloaded from http://drc.bmj.com/ on April 27, 2024 by guest. Protected by copyright.

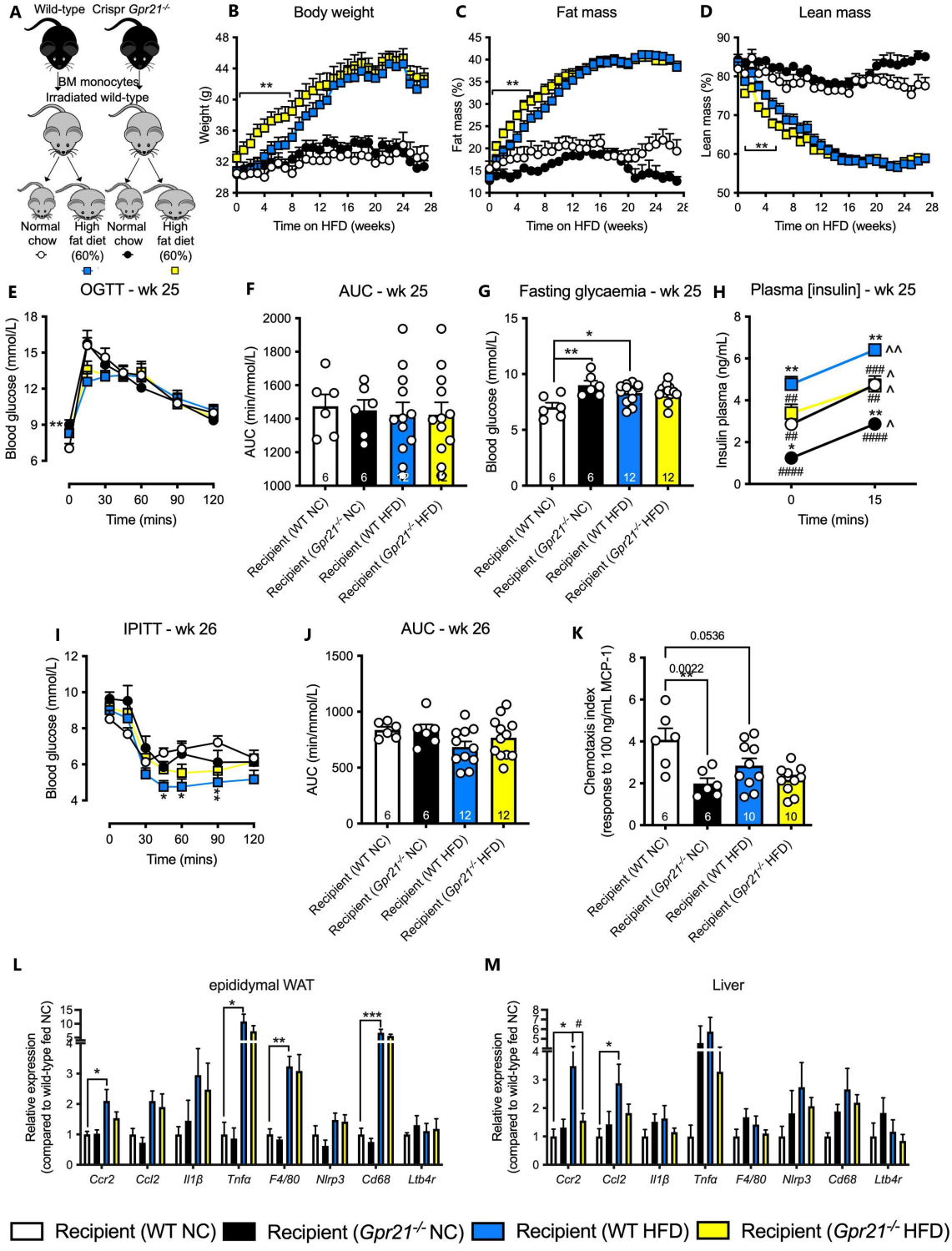

Figure 6 Bone marrow transplant (BMT) study reveals no effect on metabolic phenotype. (A) Schematic diagram of BMT study. Changes in (B) body weight (BW), (C) % fat mass, and (D) % lean mass. Week 25 (E) oral glucose tolerance test (OGTT; 3 g/kg lean), (F) area under the curve (AUC), (G) fasting glycemia, (H) plasma insulin levels (n=6–12). Week 26 (I) intraperitoneal insulin tolerance test (IPITT; 0.6 U/kg body weight for animals on normal chow (NC), or 0.75 U/kg body weight for animals fed high-fat diet (HFD)), (J) AUC. Chemotaxis of (K) $CD11b^{+}$ bone marrow (BM) monocytes isolated following completion of the BMT study from wild-type (WT) and *Gpr21*$^{-/-}$ recipient animals in response to 100 ng/mL monocyte chemoattractant protein-1 (MCP-1). Post study relative gene expression of inflammatory and energy expenditure markers in (L) epididymal white adipose tissue (WAT) and (M) liver, as measured by qPCR (*n/d*=not detected). All data are presented as mean+SEM (n=6–12, unless otherwise stated). Statistical significance was determined by two-way analysis of variance (ANOVA) with Tukey's multiple comparison test compared with wild-type NC, with *p<0.05, **p<0.01 and ***p<0.001 deemed significant, compared with wild-type HFD, with $^{\#}$p<0.05, $^{\#\#}$p<0.01, $^{\#\#\#}$p<0.001 and $^{\#\#\#\#}$p<0.0001 deemed significant, and compared with t=0 (min), with ˆp<0.05 and ˜p<0.01 deemed significant.

BMJ Open Diab Res Care: first published as 10.1136/bmjdrc-2021-002285 on 15 November 2021. Downloaded from http://drc.bmj.com/ on April 27, 2024 by guest. Protected by copyright.

increased *Ccr2* in liver was abrogated in *Gpr21*$^{-/-}$ recipient animals (figure 6L–M, n=6–12). At a cellular level, HFD significantly elevated the proportion of Ly6C^{hi} monocytes in the SVF of eWAT compared with NC-fed wild-type animals (online supplemental figure 3a–c), but this difference was lost in *Gpr21*$^{-/-}$ recipient mice. Similarly, on a NC diet, wild-type recipient mice had higher levels of Ly6C^{lo} compared with Ly6C^{hi} monocytes, a difference that was absent in *Gpr21*$^{-/-}$ recipient animals (online supplemental figure 3d,e). These data confirm that *Gpr21*$^{-/-}$ recipient mice largely retain the MCP-1/CCR2 regulatory phenotype, but not protective effects on glucose homeostasis.

DISCUSSION

There is significant debate over GPR21 as a therapeutic target for metabolic diseases. Previous studies of *Gpr21*$^{-/-}$ mice reported improvements in glucose tolerance and insulin sensitivity in mice fed HFD, putatively driven by reduced levels of metabolic tissue inflammation.[11 12] Subsequent studies ascribed this phenotype to modulation of *Rabgap1*, the gene in which *Gpr21* is nested,[13] questioning the role of GPR21 in regulating metabolism and/or inflammation.

Current therapies for T2D focus primarily on β-cell dysfunction and insulin resistance. However, the role of chemokine and cytokine-mediated chronic, low-grade inflammation in the pathophysiology of T2D and its complications has gained traction as an alternative area for therapeutic intervention.[27] Consumption of high-fat foods and reduced physical activity leads to alterations in immune cell populations. Furthermore, a significant increase in the expression levels of proinflammatory mediators, including interleukin (IL)-1β, IL-6, IL-10 and MCP-1, is routinely observed in patients with T2D,[5] shifting the balance between M2 anti-inflammatory and M1 proinflammatory macrophages. Efforts targeting this increased cytokine release have focused on neutralizing antibodies or anti-inflammatories, including anakinra (IL-1), salsalate (IKKbeta–NF-kappaB inhibition) and TNF antagonists.[28 29] This lack of efficacy is exemplified by the failure of canakinumab, an IL-1β-targeted monoclonal antibody, to reduce the incidence of new onset T2D, despite ameliorating levels of high-sensitivity C-reactive protein, and IL-6.[30 31] It remains to be seen whether a therapeutic agent focused on an 'upstream' regulator of chronic, subclinical inflammation might be more effective than targeting individual inflammatory mediators. Establishing the role of GPR21 in regulating glucose homeostasis and inflammation is thus critical to its evaluation as a potential therapeutic target.

Collectively, our findings suggest that deletion of GPR21 inhibits inflammation caused by high-fat feeding, in accordance with previous studies.[11 12] As *Rabgap1* expression was preserved in our CRISPR-Cas9 knockout mouse, the effects on inflammation and improvement in glucose homeostasis in the whole-body knockout study are likely due to *Gpr21* deletion. This contrasts with the findings of Wang *et al*,[13] who used transcription activator-like effector nucleases (TALEN) technology to generate a *Gpr21*$^{-/-}$ mouse with unperturbed *Rabgap1*, and saw no change in glucose handling. However, the report lacked a chronic HFD group and it was only after such a regimen that our study revealed the beneficial effects of *Gpr21* deletion. Furthermore, it is not clear to what extent the gene-editing methods employed might contribute to the discrepancy, beyond reported differential editing efficiencies.[32 33]

Despite the correlation observed in both clinical samples and the whole-body knockout mouse between GPR21, metabolic parameters, and inflammatory markers, the results of the BMT study suggested that effects on glucose metabolism and inflammation were not directly linked, as hematopoietic-specific deletion of GPR21 had no effect on glucose homeostasis. The most parsimonious explanation is that GPR21 regulates both monocyte-driven inflammation and glucose homeostasis, although with limited or no overlap in the mechanisms involved or functional sequelae, consistent both with previous work from our group demonstrating a decoupling of inflammation and insulin resistance[6] and the mixed literature surrounding the effects of CCR2 antagonists on glucose homeostasis.[34 35]

With our *Gpr21*$^{-/-}$ in vivo metabolic studies, deletion of *Gpr21* in cells outside of the hemopoietic lineage is required to see effects on HFD-induced changes in metabolic endpoints. Although *Gpr21* has widespread expression, a potential locus for this effect is the hypothalamus, since this tissue displays the highest expression levels of the receptor. In the original Osborn *et al*[11] study, a disconnect in body weight effect between BMT and whole-body knockout studies (similar to that observed herein) prompted the authors to silence *Gpr21* in the hypothalamus using lentiviral shRNA, leading to a modest reduction in body weight without changes in glucose homeostasis. This suggests additional, non-hemopoietic roles for GPR21 that contribute to the whole-body knockout phenotype and may enable separation between the observed improvement in glucose homeostasis and their reduced body weight. However, the role of myeloid populations in the brain cannot be excluded and would require further study, for example, with a conditional knockout mouse.

The only major difference between our BMT study and that of Osborn *et al*[11] is the method used to produce the knockout mouse. This suggests that *Rabgap1* could play an as yet unidentified role in immune cell function and glucose metabolism (expression was impaired in the original *Gpr21*$^{-/-}$ mouse). For example, *Rabgap1* is involved in the coordination of microtubule and Golgi dynamics during the cell cycle and metaphase to anaphase transition in HeLa cells.[36 37] Another explanation is that the BMT itself might protect against an insulin resistant phenotype. In a recent study, a syngeneic BMT of HFD-fed C57BL/6 mice following lethal irradiation, yielded

BMJ Open Diab Res Care: first published as 10.1136/bmjdrc-2021-002285 on 15 November 2021. Downloaded from http://drc.bmj.com/ on April 27, 2024 by guest. Protected by copyright.

reduced HFD-induced obesity, reduced adipose tissue immune cell infiltration, and decreased insulin secretion when compared with HFD control mice.[38] Furthermore, in similar studies using ob/ob mice, reduced adiposity was observed following a BMT compared with non-BMT controls,[39] perhaps highlighting a limitation of BMT in metabolic research.

The most compelling data obtained from this study was that deletion of *GPR21*, in either human and mouse monocytes, significantly decreases inflammatory chemotaxis, most notably and specifically to MCP-1, without a change in the expression of its cognate receptor, CCR2. As migration is a highly complex and tightly regulated process,[40 41] we investigated whether changes upstream of monocyte extravasation could have been disrupted. Using confocal imaging techniques, we showed that *Gpr21*$^{-/-}$ CD11b^{+} BMMs display delayed polarization in response to MCP-1. To what extent this delay is causative of reduced monocyte migration requires further investigation. However, transcriptomic analysis of *Gpr21*$^{-/-}$ CD11b^{+} BMMs revealed downregulation of key genes involved in the adhesion cascade, including *Itgb3*, *Itgax* and *VCAM*, indicative of altered extracellular matrix organization and degradation, that may play a role in the altered chemotactic responses. A comprehensive analysis of these integrin markers at the protein level, as well as monocyte interactions with endothelial cells, would be needed to further elucidate the mechanism(s) by which deletion of *Gpr21* regulates monocyte migration to MCP-1.

Intriguingly, the RNA-Seq analysis identified a number of other genes of interest. Both *Jun* and *Fos* were significantly upregulated in the *Gpr21*$^{-/-}$ CD11b^{+} BMMs. Differentiation of human PBMCs by M-CSF results in anti-inflammatory macrophages[42] and an upregulation of both *Jun* and *Fos*,[43] allowing us to speculate that *Gpr21*$^{-/-}$ CD11b^{+} BMMs might display an M2, anti-inflammatory-like phenotype and that GPR21 could be involved in suppressing chemokine expression and signaling, which correlates with the reduced effect of MCP-1. Furthermore, these data may indicate GPR21 as a potential target for the treatment of inflammatory diseases where MCP-1 and/or CCR2 has pathogenic roles, including atherosclerosis.

In summary, using a new *Gpr21* knockout mouse model, we demonstrate that whole-body deletion of the receptor ameliorates glucose intolerance induced by HFD, which is accompanied by a normalization of selected inflammatory markers. We also show that GPR21 regulates inflammatory chemotaxis in both mouse and human monocytes, likely due to altered monocyte polarization and adhesion/integrin expression and function, although a BMT study suggests that these two phenotypes are likely not linked. Finally, we describe significantly higher expression of *GPR21* in patients with T2D, which appears to correlate with CCR2 expression and function. Collectively, these data suggest that an inhibitor of GPR21 could yield improvements in both obesity-induced insulin resistance and in diseases in which CCR2-driven inflammation is a cardinal feature, opening up a number of therapeutic indications in which GPR21 antagonists might be effective.

Author affiliations
[1]Drug Discovery Biology, Monash Institute of Pharmaceutical Sciences, Parkville, Victoria, Australia
[2]Haematopoiesis and Leukocyte Biology, Baker Heart and Diabetes Institute, Melbourne, Victoria, Australia
[3]Department of Diabetes, Monash University Central Clinical School, Melbourne, Victoria, Australia
[4]Inserm UMRS 1138, Département Diabète et Endocrinologie, Sorbonne Université, Paris, France
[5]Pôle d'Innovation Thérapeutique Métabolisme, Institut de Recherches Internationales Servier, Suresnes, France

Acknowledgements AC, PMS, and MAF are/were Senior Principal Research Fellows of the Australian National Health and Medical Research Council. AJM is a CSL Centenary Fellow. Thanks to Mr Cameron Nowell for developing the scripts for the adhesion and polarization analysis (Drug Discovery Biology, Monash Institute of Pharmaceutical Sciences, Monash University, Australia).

Contributors DMR: Conceptualization, formal analysis, investigation, writing—original draft, supervision, project administration. HLK: Conceptualization, formal analysis, investigation, writing—original draft. AJM: Conceptualization, formal analysis, investigation, writing—original draft. SB-G: Investigation, formal analysis. RDIFG: Investigation, formal analysis. JM: Investigation, formal analysis. MZ: Formal analysis, data curation. SF: Resources. TLP: Investigation. ND: Investigation. PR: Investigation. AE-O: Data Curation. J-FG: Resources. NV: Resources. WNC: Writing—review and editing, funding acquisition. AC: Writing—review and editing, funding acquisition. PMS: Writing—review and editing, funding acquisition. RJS: Writing—review and editing, funding acquisition. MAF: Conceptualization, writing—review and editing. PD: Conceptualization, writing—review and editing, funding acquisition. CJL: Conceptualization, formal analysis, writing—review and editing, supervision, project administration, funding acquisition. DMR and CJL are responsible for the overall content as the guarantor.

Funding The study was funded by Servier.

Competing interests None declared.

Patient consent for publication Not applicable.

Provenance and peer review Not commissioned; internally peer reviewed.

Data availability statement All data relevant to the study are included in the article or uploaded as supplementary information.

Supplemental material This content has been supplied by the author(s). It has not been vetted by BMJ Publishing Group Limited (BMJ) and may not have been peer-reviewed. Any opinions or recommendations discussed are solely those of the author(s) and are not endorsed by BMJ. BMJ disclaims all liability and responsibility arising from any reliance placed on the content. Where the content includes any translated material, BMJ does not warrant the accuracy and reliability of the translations (including but not limited to local regulations, clinical guidelines, terminology, drug names and drug dosages), and is not responsible for any error and/or omissions arising from translation and adaptation or otherwise.

Open access This is an open access article distributed in accordance with the Creative Commons Attribution Non Commercial (CC BY-NC 4.0) license, which permits others to distribute, remix, adapt, build upon this work non-commercially, and license their derivative works on different terms, provided the original work is properly cited, appropriate credit is given, any changes made indicated, and the use is non-commercial. See: http://creativecommons.org/licenses/by-nc/4.0/.

ORCID iDs
Darren M Riddy http://orcid.org/0000-0003-0524-1498
Jon Merlin http://orcid.org/0000-0002-0062-795X

REFERENCES

1 Chawla A, Nguyen KD, Goh YPS, . Macrophage-Mediated inflammation in metabolic disease. *Nat Rev Immunol* 2011;11:738–49.

BMJ Open Diab Res Care: first published as 10.1136/bmjdrc-2021-002285 on 15 November 2021. Downloaded from http://drc.bmj.com/ on April 27, 2024 by guest. Protected by copyright.

2 Donath MY, Shoelson SE. Type 2 diabetes as an inflammatory disease. *Nat Rev Immunol* 2011;11:98–107.
3 Olefsky JM, Glass CK. Macrophages, inflammation, and insulin resistance. *Annu Rev Physiol* 2010;72:219–46.
4 Shu CJ, Benoist C, Mathis D. The immune system's involvement in obesity-driven type 2 diabetes. *Semin Immunol* 2012;24:436–42.
5 Krinninger P, Ensenauer R, Ehlers K, *et al*. Peripheral monocytes of obese women display increased chemokine receptor expression and migration capacity. *J Clin Endocrinol Metab* 2014;99:2500–9.
6 Kraakman MJ, Kammoun HL, Allen TL, *et al*. Blocking IL-6 trans-signaling prevents high-fat diet-induced adipose tissue macrophage recruitment but does not improve insulin resistance. *Cell Metab* 2015;21:403–16.
7 Maiorino MI, Bellastella G, Giugliano D, *et al*. Cooling down inflammation in type 2 diabetes: how strong is the evidence for cardiometabolic benefit? *Endocrine* 2017;55:360–5.
8 Riddy DM, Delerive P, Summers RJ, *et al*. G protein-coupled receptors targeting insulin resistance, obesity, and type 2 diabetes mellitus. *Pharmacol Rev* 2018;70:39–67.
9 Graaf Cde, Donnelly D, Wootten D, *et al*. Glucagon-Like peptide-1 and its class B G protein-coupled receptors: a long March to therapeutic successes. *Pharmacol Rev* 2016;68:954–1013.
10 Regard JB, Sato IT, Coughlin SR. Anatomical profiling of G protein-coupled receptor expression. *Cell* 2008;135:561–71.
11 Osborn O, Oh DY, McNelis J, *et al*. G protein-coupled receptor 21 deletion improves insulin sensitivity in diet-induced obese mice. *J Clin Invest* 2012;122:2444–53.
12 Gardner J, Wu S, Ling L, *et al*. G-Protein-Coupled receptor GPR21 knockout mice display improved glucose tolerance and increased insulin response. *Biochem Biophys Res Commun* 2012;418:1–5.
13 Wang J, Pan Z, Baribault H, *et al*. Gpr21 KO mice demonstrate no resistance to high fat diet induced obesity or improved glucose tolerance. *F1000Res* 2016:1–9.
14 Fan R, Toubal A, Goñi S, SGN i, *et al*. Loss of the co-repressor GPS2 sensitizes macrophage activation upon metabolic stress induced by obesity and type 2 diabetes. *Nat Med* 2016;22:780–91.
15 Gaborit B, Julla J-B, Besbes S, *et al*. Glucagon-Like peptide 1 receptor agonists, diabetic retinopathy and angiogenesis: the AngioSafe type 2 diabetes study. *J Clin Endocrinol Metab* 2020;105:e1549–60.
16 Riddy DM, Goy E, Delerive P, *et al*. Comparative genotypic and phenotypic analysis of human peripheral blood monocytes and surrogate monocyte-like cell lines commonly used in metabolic disease research. *PLoS One* 2018a;13:e0197177.
17 Lorenowicz MJ, van Gils J, de Boer M, *et al*. Epac1-Rap1 signaling regulates monocyte adhesion and chemotaxis. *J Leukoc Biol* 2006;80:1542–52.
18 Winter C, Silvestre-Roig C, Ortega-Gomez A, *et al*. Chrono-pharmacological targeting of the CCL2-CCR2 axis ameliorates atherosclerosis. *Cell Metab* 2018;28:175–82.
19 Jiang H, Lei R, Ding S-W, *et al*. Skewer: a fast and accurate adapter trimmer for next-generation sequencing paired-end reads. *BMC Bioinformatics* 2014;15:182.
20 Dobin A, Davis CA, Schlesinger F, *et al*. Star: ultrafast universal RNA-seq aligner. *Bioinformatics* 2013;29:15–21.
21 Li H, Durbin R. Fast and accurate short read alignment with Burrows-Wheeler transform. *Bioinformatics* 2009;25:1754–60.
22 Robinson MD, McCarthy DJ, Smyth GK. edgeR: a Bioconductor package for differential expression analysis of digital gene expression data. *Bioinformatics* 2010;26:139–40.
23 Subramanian A, Kuehn H, Gould J, *et al*. GSEA-P: a desktop application for gene set enrichment analysis. *Bioinformatics* 2007;23:3251–3.
24 Fabregat A, Jupe S, Matthews L, *et al*. The Reactome pathway knowledgebase. *Nucleic Acids Res* 2018;46:D649–55.
25 Subramanian A, Tamayo P, Mootha VK, *et al*. Gene set enrichment analysis: a knowledge-based approach for interpreting genome-wide expression profiles. *Proc Natl Acad Sci U S A* 2005;102:15545–50.
26 Yang J, Zhang L, Yu C, *et al*. Monocyte and macrophage differentiation: circulation inflammatory monocyte as biomarker for inflammatory diseases. *Biomark Res* 2014;2:1.
27 Xu L, Kitade H, Ni Y, *et al*. Roles of chemokines and chemokine receptors in obesity-associated insulin resistance and nonalcoholic fatty liver disease. *Biomolecules* 2015;5:1563–79.
28 Esser N, Paquot N, Scheen AJ. Anti-Inflammatory agents to treat or prevent type 2 diabetes, metabolic syndrome and cardiovascular disease. *Expert Opin Investig Drugs* 2015;24:283–307.
29 Tsalamandris S, Antonopoulos AS, Oikonomou E, *et al*. The role of inflammation in diabetes: current concepts and future perspectives. *Eur Cardiol* 2019;14:50–9.
30 Ridker PM, Howard CP, Walter V, *et al*. Effects of interleukin-1β inhibition with canakinumab on hemoglobin A1c, lipids, C-reactive protein, interleukin-6, and fibrinogen: a phase IIb randomized, placebo-controlled trial. *Circulation* 2012;126:2739–48.
31 Everett BM, Donath MY, Pradhan AD, *et al*. Anti-Inflammatory therapy with canakinumab for the prevention and management of diabetes. *J Am Coll Cardiol* 2018;71:2392–401.
32 Nerys-Junior A, Braga-Dias LP, Pezzuto P, *et al*. Comparison of the editing patterns and editing efficiencies of TALEN and CRISPR-Cas9 when targeting the human CCR5 gene. *Genet Mol Biol* 2018;41:167–79.
33 Zhang J, Liu J, Yang W, *et al*. Comparison of gene editing efficiencies of CRISPR/Cas9 and TALEN for generation of Mstn knock-out Cashmere goats. *Theriogenology* 2019;132:1–11.
34 Weisberg SP, Hunter D, Huber R, *et al*. Ccr2 modulates inflammatory and metabolic effects of high-fat feeding. *J Clin Invest* 2006;116:115–24.
35 Gale JD, Gilbert S, Blumenthal S, *et al*. Effect of PF-04634817, an oral CCR2/5 chemokine receptor antagonist, on albuminuria in adults with overt diabetic nephropathy. *Kidney Int Rep* 2018;3:1316–27.
36 Cuif MH, Possmayer F, Zander H, *et al*. Characterization of GAPCenA, a GTPase activating protein for Rab6, part of which associates with the centrosome. *Embo J* 1999;18:1772–82.
37 Miserey-Lenkei S, Couëdel-Courteille A, Del Nery E, *et al*. A role for the Rab6A' GTPase in the inactivation of the Mad2-spindle checkpoint. *Embo J* 2006;25:278–89.
38 Katiraei S, Hoving LR, van Beek L, *et al*. BMT decreases HFD-induced weight gain associated with decreased preadipocyte number and insulin secretion. *PLoS One* 2017;12:e0175524.
39 Ablamunits V, Weisberg SP, Lemieux JE, *et al*. Reduced adiposity in ob/ob mice following total body irradiation and bone marrow transplantation. *Obesity* 2007;15:1419–29.
40 Vicente-Manzanares M, Sánchez-Madrid F. Role of the cytoskeleton during leukocyte responses. *Nat Rev Immunol* 2004;4:110–22.
41 Gerhardt T, Ley K. Monocyte trafficking across the vessel wall. *Cardiovasc Res* 2015;107:321–30.
42 Hamilton TA, Zhao C, Pavicic PG, *et al*. Myeloid colony-stimulating factors as regulators of macrophage polarization. *Front Immunol* 2014;5:554.
43 Nakamura T, Datta R, Kharbanda S, *et al*. Regulation of Jun and Fos gene expression in human monocytes by the macrophage colony-stimulating factor. *Cell Growth Differ* 1991;2:267–72.

BMJ Open Diab Res Care: first published as 10.1136/bmjdrc-2021-002285 on 15 November 2021. Downloaded from http://drc.bmj.com/ on April 27, 2024 by guest. Protected by copyright.